Facile Synthesis of Mesoporous Cu2O Microspheres with Improved Catalytic Property for Dimethyldichlorosilane Synthesis

ARTICLE *in* INDUSTRIAL & ENGINEERING CHEMISTRY RESEARCH · JANUARY 2012

Impact Factor: 2.59 · DOI: 10.1021/ie2020747

I&EC research
Industrial & Engineering Chemistry Research

ARTICLE

pubs.acs.org/IECR

Facile Synthesis of Mesoporous Cu_2O Microspheres with Improved Catalytic Property for Dimethyldichlorosilane Synthesis

Zailei Zhang,[†,‡] Hongwei Che,[†] Yingli Wang,[†] Jiajian Gao,[†] Lirun Zhao,[†] Xilin She,[‡] Jin Sun,[‡] Poernomo Gunawan,[§] Ziyi Zhong,[§] and Fabing Su*[,†]

[†]State Key Laboratory of Multiphase Complex Systems, Institute of Process Engineering, Chinese Academy of Sciences, Beijing 100190, China

[‡]College of Chemical and Environmental Engineering, Qingdao University, Qingdao 266071, China

[§]Institute of Chemical Engineering and Sciences, A*star, 1 Pesek Road, Jurong Island 627833, Singapore

ABSTRACT: Mesoporous Cu_2O (MP-Cu_2O) microspheres were prepared via a facile template-free hydrothermal synthesis in the open system, in which copper acetate was used as the copper precursor and glucose as a reducing agent. The synthesis conditions and catalytic property of MP-Cu_2O for dimethyldichlorosilane synthesis via the Rochow reaction were investigated, and the formation mechanism of MP-Cu_2O microspheres was proposed. The samples were characterized by nitrogen adsorption, X-ray diffraction, temperature-programmed reduction, thermogravimetric analysis, transmission electron microscopy, and scanning electron microscopy. It was found that the synthesis conditions such as reaction temperature, time, and reactant amount added have a significant effect on the morphology and pore structure of MP-Cu_2O microspheres, and MP-Cu_2O microspheres were formed through assembly of Cu_2O nanoparticles. MP-Cu_2O microspheres with a surface area of 65.8 m^2/g, pore size of 26.7 nm, and a diameter of 400−700 nm were obtained under the optimized condition. As compared to the nonporous Cu_2O microspheres, MP-Cu_2O microspheres showed a better catalytic performance in dimethyldichlorosilane synthesis due to their developed pore structure and high surface area, which allow larger contact interface among the reaction gas, solid catalyst, and the solid reactant, together with enhanced mass transport. The work would be helpful for developing novel structured copper catalysts for organosilane synthesis and for understanding the catalytic mechanism.

1. INTRODUCTION

The synthesis of transition metal oxides with good control on their morphologies, size, and crystallographic structure has attracted much attention in recent years because these parameters significantly influence the physical and chemical properties of these materials.[1−5] Cuprous oxide (Cu_2O) is an interesting transition metal oxide that has been widely applied in gas sensor,[6] solar cells,[7] photocatalysis,[8] biosensor,[9] and lithium-ion batteries.[10] Recently, various methods have been developed for synthesizing Cu_2O with different nanostructures. For examples, interior multilayer structures of Cu_2O shell-in-shell nanoparticles were prepared in the presence of polyvinylpyrrolidone (PVP).[11] Hollow Cu_2O spheres were synthesized in an aqueous solution at room temperature using PVP as the surfactant[9] or using a multiple emulsion (O/W/O) as a template,[12] or by reducing a copper acetate solution with hydrazine in 2-propanol under reflux conditions,[13] or by a solvothermal method conducted between 150 and 180 °C for 20−40 h in *N*,*N*-dimethylformamide,[14] or by a wet-chemical method in the assistance of poly(ethylene glycol).[15] Multishelled hollow spheres of Cu_2O were also synthesized using CTAB multilamellar vesicles at 60 °C,[16] while porous Cu_2O composite hollow microspheres were obtained with high-temperature hydrothermal method,[17] and Cu_2O nanocubes with PVP in 1,5-pentanediol at 240 °C.[10] Other nanostructures of Cu_2O such as nanothreads, nanowires, and nanocubes were also synthesized by simple electrolysis-based oxidation of copper.[18] Sub-10 nm Cu_2O nanowires were obtained using an electrodeposition method assisted by PVP.[19] In addition, some methods for the preparation of Cu_2O crystals with particular morphologies were reported, including perfectly mixed 26-facet and 18-facet polyhedra of Cu_2O microcrystals synthesized by a hydrothermal process using stearic acid as a structure-directing agent,[8] and monodisperse truncated cubic, cuboctahedral, truncated octahedral, and octahedral cuprous oxide nanocrystals in an aqueous solution containing sodium dodecyl sulfate (SDS).[20] Xu et al.[21] synthesized octahedral Cu_2O crystals with tunable edge length by reducing copper hydroxide with hydrazine. Jimenez et al.[22] prepared Cu_2O bipyramids by reduction of $Cu(OH)_2$ using hydrazine as reducing agent. Highly uniform monodisperse Cu_2O nanocrystals were synthesized in a solution containing oleic acid and trioctylamine at 180 °C.[23] From these literature results, it is found that, to obtain morphology-controllable nanostructures of Cu_2O, expensive template, toxic reducing agent, high reaction temperatures and pressures, as well as long reaction time are often applied. Therefore, it is required to develop facile methods to fabricate novel Cu_2O nanostructures for practical applications.

It has been reported that metallic copper[24] and its compounds such as Cu_2O,[25] CuO,[25] CuCl,[26] Cu_3Si,[27] and Cu−Cu_2O−CuO composite[28] mixed with promoter additives[29] were active for Rochow reaction. This direct synthesis of methylchlorosilanes

Received: September 10, 2011
Accepted: December 22, 2011
Revised: November 30, 2011
Published: December 22, 2011

dx.doi.org/10.1021/ie2020747 | *Ind. Eng. Chem. Res.* 2012, 51, 1264–1274

(MCS) using silicon to react with chloromethane (MeCl) over the copper catalysts is still the most economical route to MCS in organosilane industry. In this reaction, the main products are methyltrichlorosilane (CH_3SiCl_3, M1), dimethyldichlorosilane ($(CH_3)_2SiCl_2$, M2), and trimethylchlorosilane ($(CH_3)_3SiCl$, M3), and among them M2 is highly desired as the organosilane monomer to synthesize organosilicon products in industry. Thus, the selectivity for M2 is the top priority in industrial production. Because this reaction involves complex gas−solid−solid phase catalysis together with many byproducts, many efforts have been made to develop efficient copper catalysts and to investigate its catalytic mechanism.[26,31,32] In general, the copper catalysts used in organosilane industry[33] and academic research[34,35] have dense structures with irregular morphology and micrometer sized particles. Furthermore, it is well-known that porous catalysts with high surface-to-volume ratios often result in enhanced catalytic activity.[36−38] Therefore, it is necessary to prepare novel porous copper catalysts for organosilane synthesis, which have yet been developed.

Herein, we report the preparation and characterization of mesoporous Cu_2O (MP-Cu_2O) microspheres as catalysts for the Rochow reaction. The facile template-free hydrothermal synthesis method employed here is conducted at the mild condition in the open system and is easily scaled up. MP-Cu_2O obtained under the optimized condition possesses a mesoporous structure with a high surface area and a particle size at micrometer level. The catalytic performance of MP-Cu_2O microspheres for M2 synthesis was then investigated. As compared to the nonporous Cu_2O (NP-Cu_2O) microspheres, MP-Cu_2O microspheres exhibit better catalytic performance with higher M2 selectivity and Si conversion. This may arise from the creation of more active species Cu_3Si due to abundant pore structure of MP-Cu_2O, which could lead to more contact interface among gas MeCl, solid catalyst, and solid Si, as well as enhanced gas transportation within the pore system. Our work would be helpful for developing novel porous Cu catalysts and understanding the catalytic mechanism.

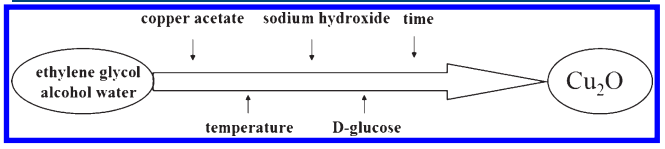

Figure 1. Scheme of synthesis process.

2. EXPERIMENTAL SECTION

2.1. Material Synthesis. Cu_2O microspheres were prepared by a hydrothermal method as shown in Figure 1. To optimize the synthesis condition and investigate the product formation mechanism, the synthesis parameters such as the reaction temperature, time, and reactant amount were varied, which are listed in Table 1. In a typical synthesis (sample S3 in Table 1), 10.0 mL of deionized water, 50.0 mL of absolute alcohol (CH_3CH_2OH, A.R., Sinopharm Chemical Reagent Co., Ltd.), and 20.0 mL of ethylene glycol ($C_2H_6O_2$, A.R., Sinopharm Chemical Reagent Co., Ltd.) were mixed to form a solution in a beaker, into which 1.00 g of copper acetate ($Cu(CH_3COO)_2 \cdot H_2O$, A.R., Sinopharm Chemical Reagent Co., Ltd.) was added. The solution was heated to 70 °C under stirring, followed by the addition of 1.40 g of sodium hydroxide (NaOH, A.R., Sinopharm Chemical Reagent Co., Ltd.) and 1.20 g of D-glucose ($C_6H_{12}O_6 \cdot H_2O$, A.R., Sinopharm Chemical Reagent Co., Ltd.). After being stirred for 30 min at 70 °C, the beaker was cooled to room temperature. The resulting precipitate solid was collected by centrifugation, washed with distilled water and pure ethanol, and finally dried in a vacuum at 60 °C for 8 h.

2.2. Characterization. X-ray diffraction (XRD) patterns were recorded on a PANalytical X'Pert PRO MPD using the Kα radiation of Cu (λ = 1.5418 Å). The crystal size of the sample was calculated using the Debye−Scherrer equation. The microscopic feature of the samples was observed by field-emission scanning electron microscopy (SEM) (JSM-6700F, JEOL, Tokyo, Japan) and transmission

Table 1. Synthesis Conditions Used for Preparing Cu_2O Microspheres

sample	DI-water (mL)	ethanol (mL)	glycol (mL)	copper acetate (g)	sodium hydroxide (g)	glucose (g)	reaction T (°C)	reaction t (min)	surface area (m^2/g)
S1	10	50	20	1.00	1.40	1.20	50	30	49.8
S2	10	50	20	1.00	1.40	1.20	60	30	56.7
S3	10	50	20	1.00	1.40	1.20	70	30	65.8
S4	10	50	20	1.00	1.40	1.20	80	30	44.8
S5	10	50	20	1.00	1.40	1.20	90	30	45.0
S6	10	50	20	1.00	1.40	1.20	100	30	32.7
S7	10	50	20	1.00	1.40	1.20	70	10	37.4
S8	10	50	20	1.00	1.40	1.20	70	60	15.2
S9	10	50	20	1.00	1.40	1.20	70	300	5.0
S10	10	50	20	1.00	1.40	1.20	70	600	5.2
S11	10	50	20	0.20	1.40	1.20	70	30	5.1
S12	10	50	20	0.50	1.40	1.20	70	30	28.6
S13	10	50	20	2.00	1.40	1.20	70	30	16.6
S14	10	50	20	1.00	0.28	1.20	70	30	6.4
S15	10	50	20	1.00	0.70	1.20	70	30	4.6
S16	10	50	20	1.00	2.80	1.20	70	30	38.6
S17	10	50	20	1.00	1.40	0.20	70	30	23.6
S18	10	50	20	1.00	1.40	0.60	70	30	36.7
S19	10	50	20	1.00	1.40	2.40	70	30	1.8
S20	10	50	20	2.00	2.80	2.40	70	30	58.9

dx.doi.org/10.1021/ie2020747 |Ind. Eng. Chem. Res. 2012, 51, 1264–1274

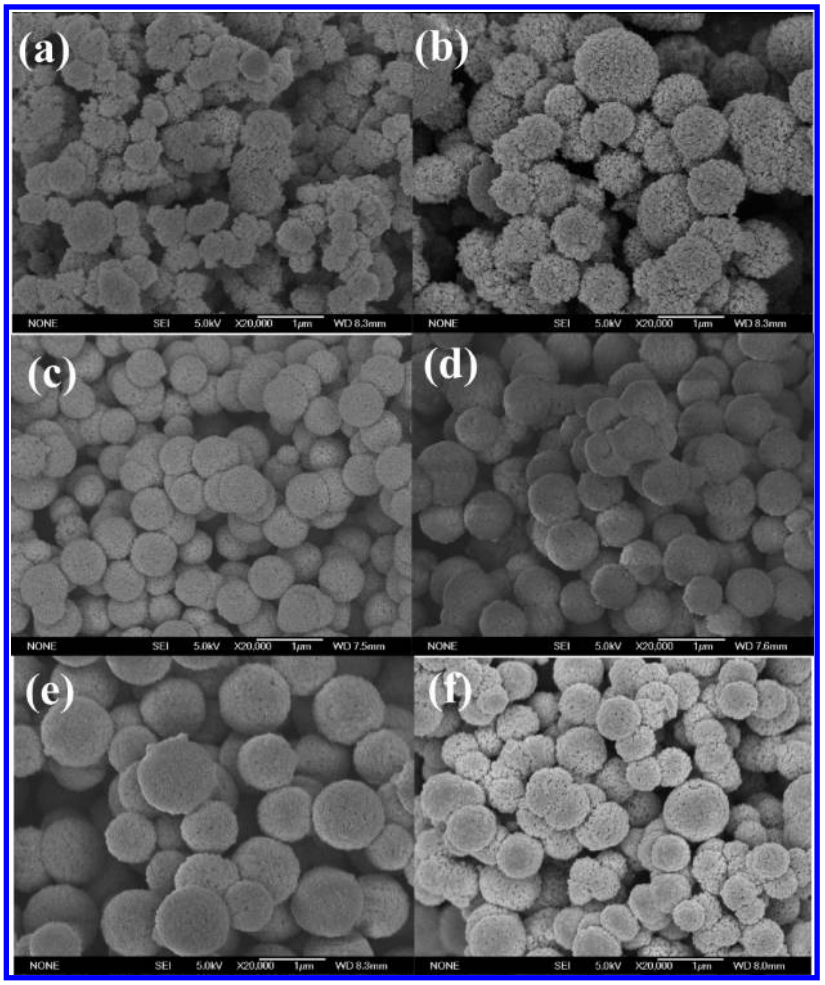

Figure 2. SEM images of Cu_2O microspheres obtained at different reaction temperatures: (a) 50 °C (S1), (b) 60 °C (S2), (c) 70 °C (S3), (d) 80 °C (S4), (e) 90 °C (S5), and (f) 100 °C (S6).

electron microscopy (TEM) (JEM-2010F, JEOL,Tokyo, Japan). The pore nature of the samples was investigated using physical adsorption of N_2 at the liquid-nitrogen temperature (−196 °C) on an automatic volumetric sorption analyzer (NOVA3200e, Quantachrome). Prior to the measurement, the sample was degassed at 200 °C for 5 h under vacuum. The specific surface area was determined according to the Brunauer−Emmett−Teller (BET) method in the relative pressure range of 0.05−0.2. Pore size distribution (PSD) curve was derived from the Barrett−Joyner−Halenda (BJH) method using adsorption branch. The pore size was estimated from the maximum position of the BJH-PSD curve. Thermal gravimetric (TG) analysis was carried out on a EXSTAR TG/DTA 6300 instrument (Seiko Instruments, Japan) with a heating rate of 5 °C/min in air (200 mL/min). Temperature programmed reduction (TPR) measurements were carried out on automated chemisorption analyzer (ChemBET pulsar TPR/TPD, Quantachrome). Upon loading of 0.10 g of Cu_2O microspheres into a quartz U-tube, the sample was degassed at 200 °C for 30 min under helium. When the temperature dropped to 20 °C, the gas was changed to 9.9% H_2/Ar. Finally, the sample was heated from 20 to 800 °C with 10 °C/min in 9.9% H_2/Ar with a gas flow of 30 mL/min.

2.3. Measurement of Catalytic Property. The evaluation of catalyst was carried out with a typical MCS lab fixed-bed reactor.[25] 10.00 g of Si powder (20−50 mesh, provided by Jiangsu Hongda New Material Co., Ltd.) and 1.00 g of MP-Cu_2O or NP-Cu_2O together with 0.10 g of Zinc (Zn, A.R., Sinopharm Chemical Reagent Co., Ltd.) used as a promoter were mixed homogeneously to form a contact mass, which was then loaded in the glass reactor. The reactor system was purged with purified N_2 for 0.5 h followed by heating to 325 °C (or 345 °C) within 1 h under a N_2 flow rate of 25 mL/min. Subsequently, N_2 was turned off, and MeCl gas with a flow rate of 25 mL/min was introduced into the reactor to react with Si at 325 °C (or 345 °C). After a given period of 24 h, the reaction was stopped. The gas product was cooled to liquid with the circulator bath controlled at 5 °C by a programmable thermal circulator (GDH series, Ningbo xinzhi biological technology Co., LTD). The waste contact mass (solid residue after reaction) containing unreacted Si powder and Cu+Zn compounds was weighed for calculating Si conversion. The liquid phase collected in a glass container was analyzed with an Agilent Technologies 7890A GC system. The Rochow reaction was shown in formula 1 as follows:

$$\mathrm{Si + MeCl} \xrightarrow[300\text{-}350\ ^\circ\mathrm{C}]{\text{copper catalyst}} \begin{array}{l}(CH_3)_3SiCl\\(CH_3)_2SiCl_2\\CH_3SiCl_3\\CH_3HSiCl_2\\(CH_3)_2HSiCl\\\text{other low boilers}\\\text{residue}\end{array} \quad (1)$$

The main MCS products are M1, M2, and M3, which normally account for ≥95 wt % of the total reaction product amount.[33]

dx.doi.org/10.1021/ie2020747 |*Ind. Eng. Chem. Res.* 2012, 51, 1264–1274

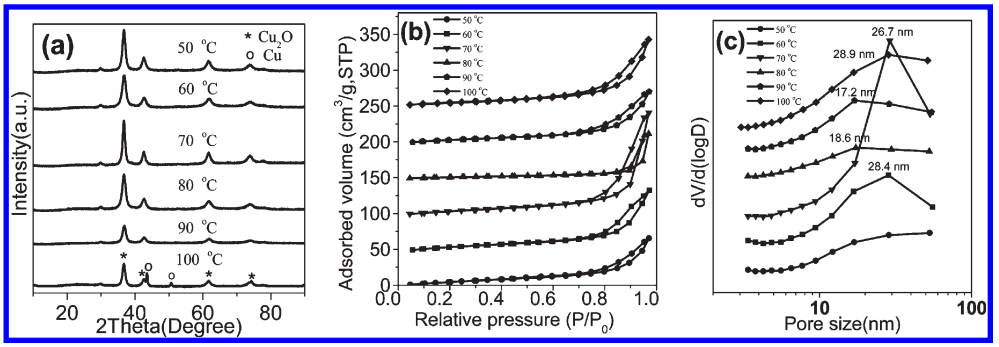

Figure 3. XRD patterns (a), N_2 adsorption−desorption isotherms (b), and BJH-PSD curves (c) of Cu_2O microspheres obtained at different reaction temperatures: 50 °C (S1), 60 °C (S2), 70 °C (S3), 80 °C (S4), 90 °C (S5), and 100 °C (S6). (For clarity, the isotherm of S2, S3, S4, S5, and S6 was vertically shifted for 50, 100, 150, 200, and 250 cm^3/g, respectively.)

Thus, to simplify the calculation, other trace products and the change of catalyst weight were ignored. The formulas for calculation of the selectivity of M*i* (*i* = 1, 2, 3) and S*i* conversion are given below:

$$\text{selectivity of Mi } (S_{\text{Mi}}) = \frac{\text{mole}_{Mi}}{\sum_{i=1}^{3} \text{mole}_{Mi}} \times 100\% (i = 1, 2, 3) \quad (2)$$

$$\text{conversion of Si } (C_{Si}) = \frac{\text{weight}_{\text{contact mass before reaction}} - \text{weight}_{\text{contact mass after reaction}}}{\text{weight}_{\text{Si before reaction}}} \times 100\% \quad (3)$$

3. RESULTS AND DISCUSSION

Previous work has demonstrated that the parameters for synthesizing nanostructured Cu_2O such as temperature,[11] time,[39] and reactant concentration[40] have strong effects on the morphology and pore structure of the products. Therefore, to obtain MP-Cu_2O microspheres with high surface area and uniform morphology, we systematically investigated these parameters, and on the basis of the experimental results, we proposed a formation mechanism of MP-Cu_2O microspheres.

3.1. Effect of the Reaction Temperature. Figure 2 shows the SEM images of Cu_2O microspheres obtained at different reaction temperatures. It can be seen that sample S1 in Figure 2a obtained at 50 °C has nonuniform microspherical morphology with a size distribution of 100−1000 nm, and the microspheres are composed of nanoparticles with several tenth of nanometers in size, which act as the building block units. Similar results are observed for the samples obtained at 60, 70, 80, 90, and 100 °C (S2−S6 in Table 1), respectively, which are all microspheres with relatively uniform morphology and constructed with small nanoparticles of 20−50 nm in size. However, when the reaction temperature reaches 100 °C, the obtained sample S6 has a less uniform particle size distribution as compared to those of the S3, S4, and S5 samples. It should be mentioned that at this temperature, the main product is Cu_2O nanoparticles with a low yield after filtration (15% of Cu added). Hence, we can conclude that the microspheres are assembled with Cu_2O nanoparticles and the reaction temperature between 70 and 90 °C should be suitable for the preparation of homogeneous Cu_2O microspheres.

Figure 3a shows the XRD patterns of the samples obtained at different temperatures. Diffraction peaks at 2θ values of 29.7°, 36.7°, 42.7°, 61.6°, and 73.5° are observed, which correspond to the lattice plane of (110), (111), (200), (220), and (311), respectively, of Cu_2O, indicating the presence of the pure cubic symmetry Cu_2O (JCPDS no. 05-0667). However, at the reaction temperature of 100 °C, in addition to the Cu_2O phase, a small amount of metallic Cu is also observed. This phenomenon will be investigated later. Using the Debye−Scherrer formula based on the peak at 36.7°, the average Cu_2O crystal size is calculated to be 10.8, 12.7, 15.0, 15.8, 19.1, and 21.3 nm for the samples obtained at 50, 60, 70, 80, 90, and 100 °C, respectively, suggesting that higher synthesis temperatures result in larger Cu_2O nanocrystals.

Figure 3b presents N_2 adsorption/desorption isotherms of the samples prepared at 50 °C (S1), 60 °C (S2), 70 °C (S3), 80 °C (S4), 90 °C (S5), and 100 °C (S6). These isotherms with a hysteresis loop in the relative pressure range of 0.7−1.0 belong to the type IV. The BET surface areas for S1−S6 are 49.8, 56.7, 65.8, 44.8, 45.0, and 32.7 m^2/g, respectively. The PSD curves in Figure 3c show that the pore size distributions at the maxima for S2−S6 are 28.4, 26.7, 18.6, 17.2, and 28.9 nm, respectively, suggesting mesoporous structure. In contrast, the pore size for S1 is larger than 50 nm, beyond the mesoporous range. The surface area of these samples should be derived from the surface of these building block nanoparticles, and the formed pores can be from the interspaces of the constituent nanoparticles as observed in above SEM images. As S3 possesses the maximum surface area and highest porosity, a synthesis temperature of 70 °C will be applied in the following sample preparations.

3.2. Effect of Reaction Time. Figure 4 shows the SEM and TEM images of the Cu_2O microspheres obtained at different reaction times after adding D-glucose. Figure 4a and b shows the morphology of Cu_2O microspheres prepared at 10 min (S7 in Table 1). It can be seen from Figure 4a that the sample S7 has a spherical morphology with a diameter of 400−700 nm. These microspheres are composed of small nanoparticles of 20−50 nm in size. The TEM image in Figure 4b reveals the dense internal structure of S7. Upon further extending the reaction time to 30 min (S3 in Table 1), as shown in Figure 4c and d, there is no obvious change in morphology of S3, which still consisted of small nanoparticles, but with a little larger size and a looser packing, which leads to more internal porosity. When the reaction was prolonged to 60 min (S8 in Table 1), as can be seen in Figure 4e and f, the diameter of S8 microspheres decreases to 400−500 nm and the building block nanoparticle size increases nearly to 50−100 nm. After 300 min of reaction

dx.doi.org/10.1021/ie2020747 |*Ind. Eng. Chem. Res.* 2012, 51, 1264–1274

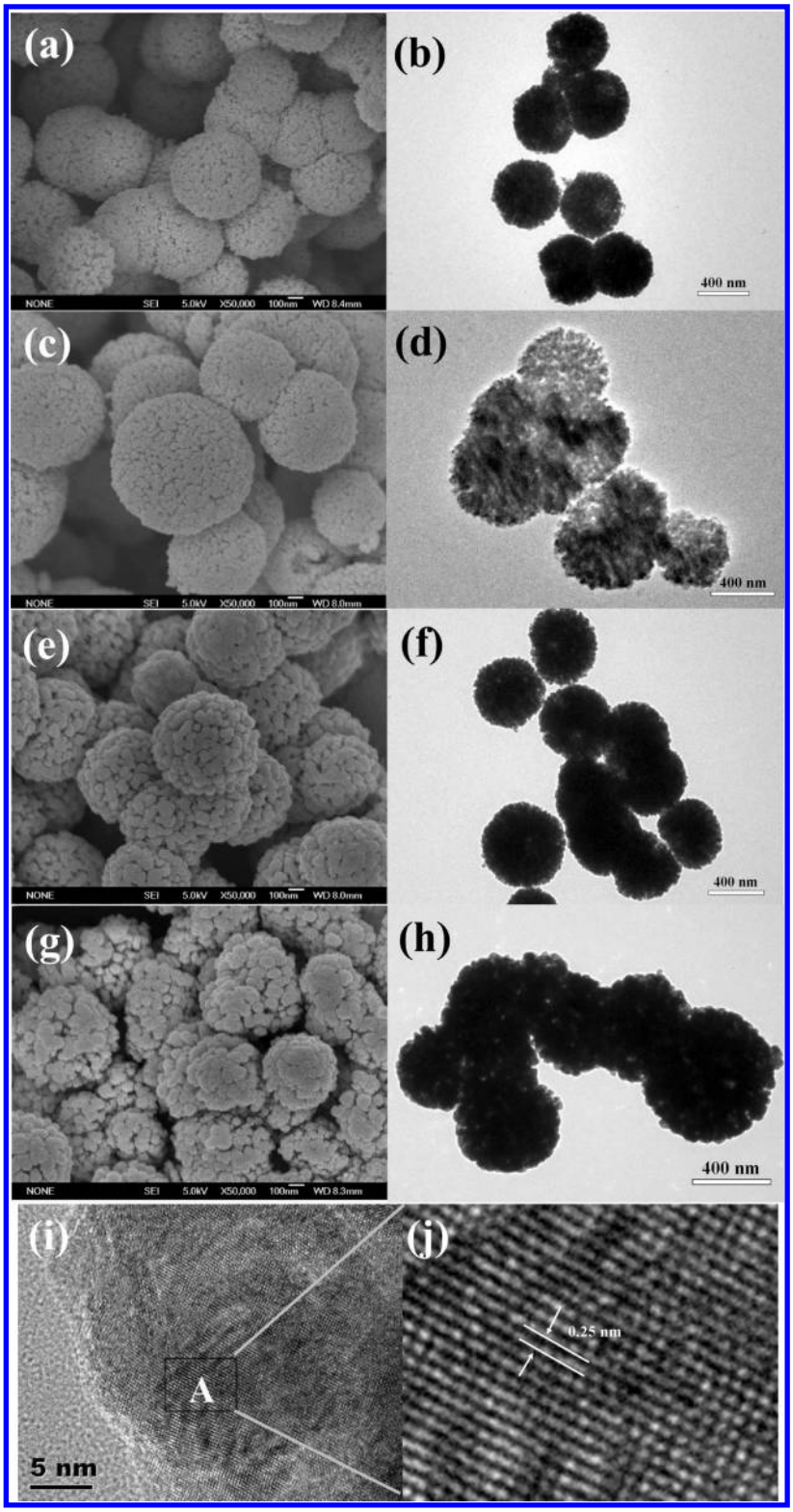

Figure 4. SEM (left) and TEM (right) images of Cu_2O microspheres obtained at different reaction times: (a and b) 10 min (S7), (c and d) 30 min (S3), (e and f) 60 min (S8), and (g and h) 300 min (S9); (i) HRTEM image on the edge of MP-Cu_2O (S3); (j) enlarged view of area A (S3).

(S9 in Table 1), there was no obvious change as compared to S8 in morphology as shown in Figure 4g and h, but the building block nanoparticles size seems a little larger. The morphology of S10 obtained with 600 min (not shown here) has no big change as compared to S9 (300 min). Thus, as shown in Figure 4e and g, the Cu_2O nanoparticles that construct the Cu_2O microspheres gradually become larger in size with the extension of the reaction time to above 60 min. Figure 4i shows the HRTEM image on the edge of MP-Cu_2O microspheres (S3), which consist of a large number of nanocrystals that pack together in different

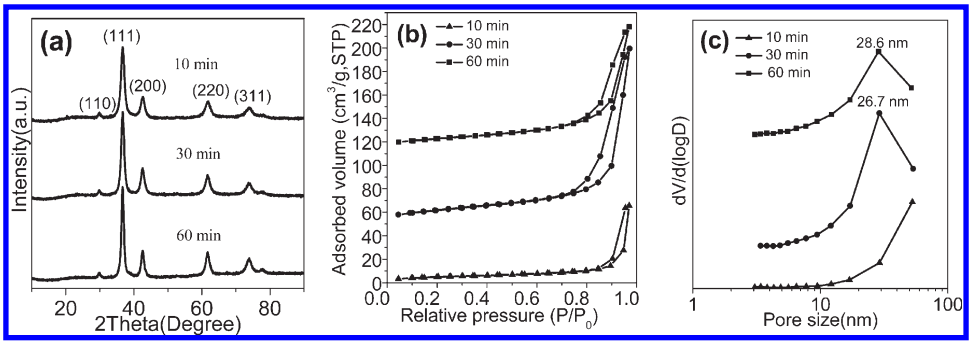

Figure 5. (a) XRD patterns, (b) N_2 adsorption−desorption isotherms, and (c) BJH-PSD curves of Cu_2O samples synthesized with different reaction times: 10 min (S7), 30 min (S3), and 60 min (S8). (For clarity, the isotherm of S3 and S8 was vertically shifted for 60 and 120 cm^3/g, respectively.)

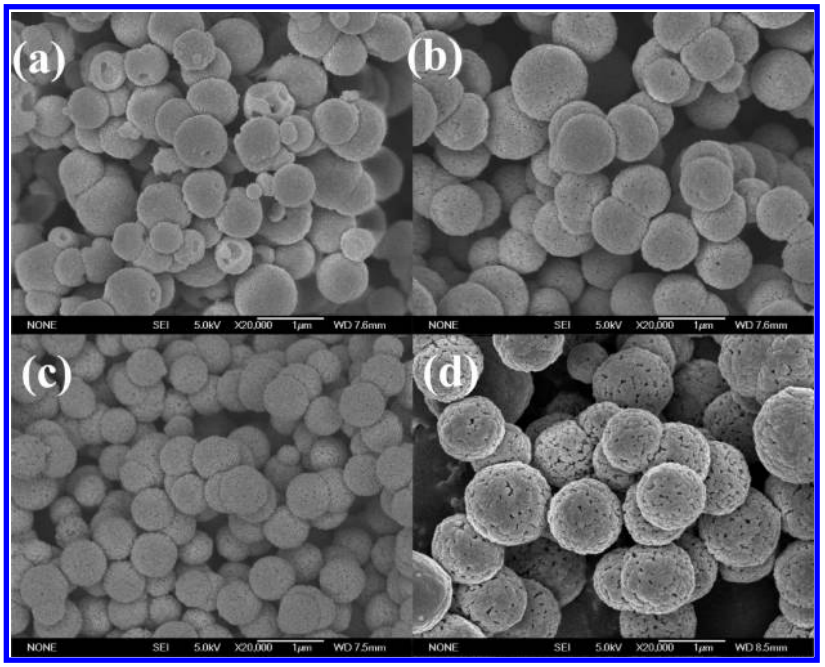

Figure 6. SEM images of the Cu_2O microspheres obtained at different copper acetate amounts: (a) 0.20 g (S11), (b) 0.50 g (S12), (c) 1.00 g (S3), and (d) 2.00 g (S13).

orientations. The enlarged view of area A in Figure 4i shows that the lattice plane distance measured is 0.25 nm, which is in agreement with the (111) plane distance of cubic Cu_2O (0.2465 nm tabulated from XRD).

Figure 5a shows XRD patterns of the Cu_2O samples prepared after 10, 30, and 60 min of reaction (S7, S3, and S8, respectively). All diffraction peaks were identified, and they suggest the presence of pure cubic symmetry Cu_2O (JCPDS no. 05-0667). Their average Cu_2O crystal sizes are calculated to be 10.1, 15.4, and 20.1 nm, respectively. The XRD patterns of S9 (300 min) and S10 (600 min) are similar to that of S8 (not shown here), with no significant difference in their average crystal size 20.2 nm. The N_2 adsorption/desorption isotherms are presented in Figure 5b, and they exhibit a hysteresis loop in the relative pressure range of 0.7−1.0, which belongs to the type IV. The BET surface areas are 37.4 m^2/g for S7, 65.8 m^2/g for S3, and 15.2 m^2/g for S8, and the PSD curves in Figure 5c demonstrate mesoporous structure for S7 and S3 but not for S8 as its pore size is larger than 50 nm. The isotherms and PSD curves for S9 (300 min) and S10 (600 min) are similar to those of S8 and are not shown here. Their surface area is around 5.0 m^2/g. Therefore, a reaction time of 30 min is selected as it leads to high porosity of the Cu_2O microspheres.

3.3. Effect of Reactant Amount. In this work, copper acetate, sodium hydroxide, and glucose were used as the reactants. The amounts added should influence the morphology and pore structure of Cu_2O microspheres. Figure 6 shows the SEM images of the Cu_2O microspheres prepared with different copper acetate amounts. It was observed that, when the amount of copper acetate is 0.20 g (S11 in Table 1), the morphology of S11 as shown in Figure 6a is nonuniform microspheres with a dense surface structure and a diameter of about 50−1000 nm. Further increasing the copper acetate amount to 0.50 g (S12 in Table 1), the microsphere size of S12 becomes 500−1000 nm as shown in Figure 6b. A large number of pores are formed on the S12 surface, resulting from the stacking of Cu_2O nanoparticles. With 1.00 g of copper acetate (S3 in Table 1), Cu_2O microspheres are formed with small pores on the surface and are relatively uniform, as

dx.doi.org/10.1021/ie2020747 |*Ind. Eng. Chem. Res.* 2012, 51, 1264–1274

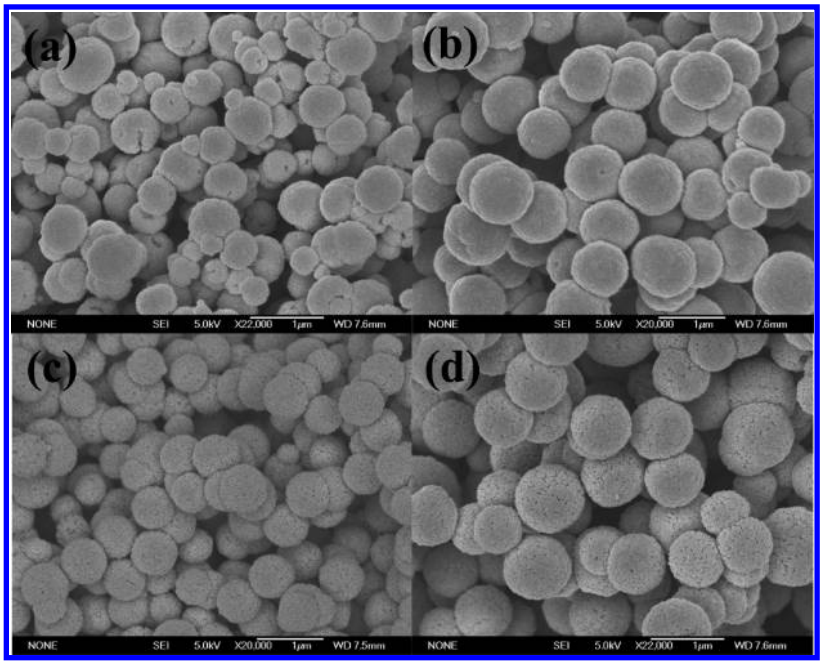

Figure 7. SEM images of the Cu_2O microspheres obtained at different sodium hydroxide amounts: (a) 0.28 g (S14), (b) 0.70 g (S15), (c) 1.40 g (S3), and (d) 2.80 g (S16).

shown in Figure 6c. Finally, with further increase of copper acetate to 2.00 g (S13 in Table 1), the obtained Cu_2O sample has the same microspherical morphology but with larger pores and building block particle size (see Figure 6d) as compared to S12 and S3 samples prepared with a lower amount. Samples S11, S12, S3, and S13 exhibit mesoporous structures with pore sizes of 28.9 (S12), 26.7 (S3), and 31.9 (S13) nm, respectively, while their BET surface areas are 5.1, 28.6, 65.8, and 16.6 m^2/g, respectively. For S11, the pore size is beyond the mesoporous level. Therefore, 1.00 g of copper acetate amounts is better for obtaining the high surface area of MP-Cu_2O microspheres.

Figure 7 reveals the SEM images of Cu_2O microspheres prepared with different sodium hydroxide amounts. When 0.28 and 0.70 g of sodium hydroxide is added (S14 and S15 in Table 1), incomplete and nonuniform Cu_2O microspheres without visible pores on their surface are obtained (Figure 7a and b), which corresponds to the small BET surface areas (6.4 and 4.6 m^2/g, respectively). With further increase to 1.40 g (S3 in Table 1) and 2.80 g (S16 in Table 1), the Cu_2O microspheres become more uniform, and a large number of small pores are created (Figure 7c and d), as supported by the increase of surface areas to 65.8 and 38.6 m^2/g, respectively. In addition, sample S16 also demonstrates mesoporous structure with a pore size of 28.5 nm. Therefore, 1.40 and 2.80 g of sodium hydroxide amounts are suitable in our work.

Figure 8 shows the SEM images of Cu_2O microspheres prepared with different glucose amounts added. When the amount of glucose is 0.24 g (S17 in Table 1) and 0.60 g (S18 in Table 1), Cu_2O microspheres with many pores on their surface are formed, and their diameter is around 1000 nm as shown in Figure 8a and b, respectively. When the glucose amount is increased to 1.20 g (S3 in Table 1), the size of the uniform Cu_2O microspheres become smaller and is between 400 and 700 nm, and pores also can be observed on their surface (Figure 8c). Further increasing the glucose amount to 2.40 g (S19 in Table 1), the size of Cu_2O microspheres becomes smaller, and the pores disappear (Figure 8d). The surface area is 23.6 m^2/g for S17, 36.7 m^2/g for S18, 65.8 m^2/g for S3, and 1.8 m^2/g for S19. The pore size at the maximum position derived from BJH method is 30.3 nm for S17, 29.9 nm for S18, and 26.7 nm for S3, suggesting they are mesoporous. Therefore, 1.20 g of glucose amount is suitable for obtaining the desirable MP-Cu_2O microspheres.

In short, MP-Cu_2O microspheres can be synthesized under a relatively wide synthetic condition, of which the optimized condition is that used for S3 (see Table 1). We also investigated the possibility of scaling up the production by doubling the amount of all of the reactants used for S3 (S20 in Table 1) and found that S20 has microspherical morphology and surface area similar to those of S3, implying the synthesis method is scalable for mass production.

3.4. Proposed Synthesis Process of MP-Cu_2O Microspheres. The reactions involved in the formation of MP-Cu_2O microspheres are shown in eqs 4−6.

$$Cu^{2+} + 2OH^- \rightarrow Cu(OH)_2 \downarrow \quad (4)$$

$$Cu(OH)_2 + 2OH^- \rightarrow (Cu(OH)_4)^{2-} \quad (5)$$

$$2(Cu(OH)_4)^{2-} + C_6H_{12}O_6 \rightarrow Cu_2O \downarrow + C_6H_{11}O_7^- + 3OH^- + 3H_2O \quad (6)$$

Figure 9a shows the color change during the S8 synthesis process. First, 1.00 g of copper acetate was added to 80 mL of transparent solution containing water, alcohol, and glycol at 70 °C under stirring to form light blue color copper acetate solution. After addition of 1.40 g of sodium hydroxide, the solution turned deep blue quickly, indicating the formation of $(Cu(OH)_4)^{2-}$ [41] Next, 1.20 g of glucose was added, which made the solution change into a brown color, indicating the formation of the small Cu_2O nanoparticles due to fast nucleation and crystal growth.[42−44] This is inferred from the case of S1, in which brown

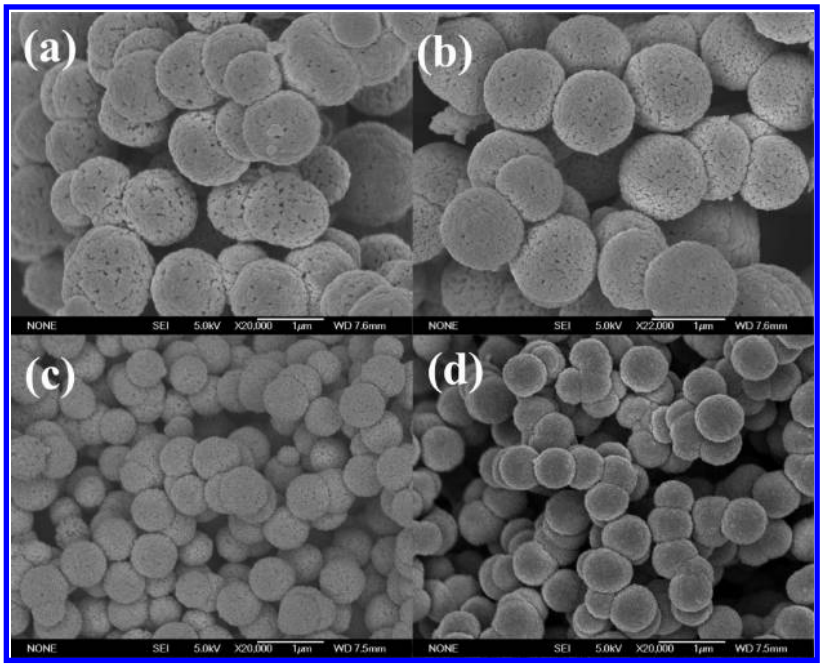

Figure 8. SEM images of the Cu_2O microspheres obtained at different glucose amounts: (a) 0.24 g (S17), (b) 0.60 g (S18), (c) 1.20 g (S3), and (d) 2.40 g (S19).

Figure 9. (a) The color change of solution during synthesis process of Cu_2O microspheres; and (b) illustration of the possible formation process of MP-Cu_2O microspheres.

filtrate and a small amount of product were obtained. Because the fresh Cu_2O nanoparticles are instable and tend to self-assemble into larger spheres for minimizing the interfacial energy,[45] with the increase of reaction time from 10 to 60 min, the solution color was changed from brown to dark brown and finally to black, and after filtration, the solution became transparent, suggesting the formation of the Cu_2O microspheres. On the basis of the above observations, a three-stage growth formation process of the MP-Cu_2O microspheres is proposed (Figure 9b). At the first stage, $(Cu(OH)_4)^{2-}$ is formed via the reaction of copper acetate and sodium hydroxide. Next, $(Cu(OH)_4)^{2-}$ is rapidly reduced by glucose to form small Cu_2O nanoparticles under stirring. At the second stage, the initially formed small nanoparticles self-assemble or aggregate into MP-Cu_2O microspheres. Subsequently, small building block nanoparticles within MP-Cu_2O transform to large ones with the extension of the reaction time through Ostwald ripening.[46] In this process, glycol absorbed on the surface of the nanoparticles may act as structure-directing agent to regulate the surface state of the nanoparticles. The surface modification of these small molecules on the surface state influences the nucleation and aggregation process of the nanoparticles, which finally lead to the formation of mesoporous structures.[47,48] When a small amount of NaOH is added (0.28 and 0.70 g), the rate of nucleation and ripening is faster, and the formed particles are encapsulated by constraining crystal grain growth after adding glucose into the solution.[49] Therefore, nonporous Cu_2O were formed as shown in Figure 7a and b (S14 and S15 in Table 1).

3.5. The Oxidability and Reducibility of MP-Cu_2O and NP-Cu_2O Microspheres. The oxidability and reducibility are important for a metal oxide catalyst. Figure 10a shows the TG curves of both MP-Cu_2O (S3 in Table 1) and NP-Cu_2O (S15 in Table 1)

dx.doi.org/10.1021/ie2020747 |*Ind. Eng. Chem. Res.* 2012, 51, 1264–1274

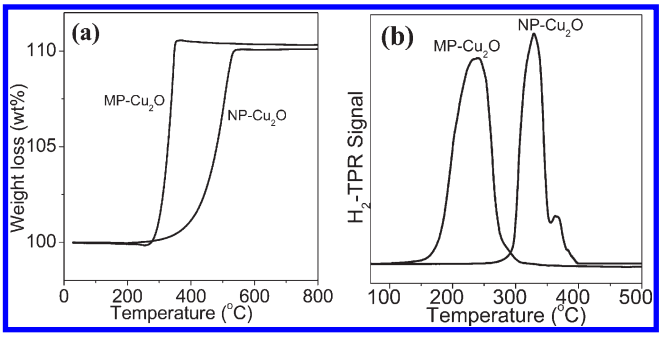

Figure 10. TG (a) and H_2-TPR (b) curves of MP-Cu_2O (S3) and NP-Cu_2O (S15).

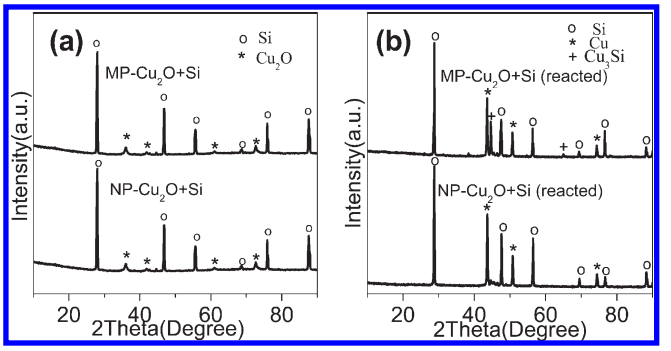

Figure 11. XRD patterns of contact masses (MP-Cu_2O and NP-Cu_2O mixed with silicon) before (a) and after (b) reaction at 345 °C.

Table 2. Catalytic Performance of Cu_2O Microspheres for the Rochow Reaction

catalyst	S_{M1} (%)	S_{M2} (%)	S_{M3} (%)	C_{Si} (%)
MP-Cu_2O (325 °C) (S3)	36.0	62.5	1.5	33.2
NP-Cu_2O (325 °C) (S15)	52.9	45.2	1.9	17.8
MP-Cu_2O (345 °C) (S3)	30.3	66.4	3.3	40.8
NP-Cu_2O (345 °C) (S15)	48.9	49.1	2.0	24.6

as representatives in air. It can be seen that the oxidation of MP-Cu_2O occurred at about 270 °C and is complete at 370 °C. In contrast, the oxidation temperature for NP-Cu_2O is in the range of 300−580 °C. The complete oxidation temperature of MP-Cu_2O is lower by 210 °C than that of NP-Cu_2O, suggesting that MP-Cu_2O is oxidized easier than NP-Cu_2O. Figure 10b shows the H_2-TPR curves of MP-Cu_2O (S3 in Table 1) and NP-Cu_2O (S15 in Table 1). For the S3 sample, the H_2 consumption peak is located at about 240 °C, while the NP-Cu_2O microspheres give a main reduction peak at about 330 °C. The maximum reduction peak for MP-Cu_2O is lower by near 100 °C than that of NP-Cu_2O, suggesting MP-Cu_2O is more reducible. These results clearly demonstrate that the MP-Cu_2O microspheres have a higher ability for both the oxidability and the reducibility than NP-Cu_2O, probably because of the much higher surface area of the former.[50]

3.6. Catalytic Property. Table 2 shows the catalytic performance of MP-Cu_2O (S3 in Table 1) and NP-Cu_2O (S15 in Table 1) as copper catalysts for Rochow reaction. It can be seen that MP-Cu_2O exhibits a higher Si conversion (C_{si}) of 33.2% at 325 °C and 40.8% at 345 °C than that of NP-Cu_2O (17.8% at 325 °C and 24.6% at 345 °C). More importantly, MP-Cu_2O shows a higher M2 selectivity (S_{M2}) of 62.5% at 325 °C and 66.4% at 345 °C than that of NP-Cu_2O (45.2% at 325 °C and 49.1% at 345 °C). As we know, a high M2 is highly desirable in organosilane industry. The results demonstrate that the synthesized MP-Cu_2O microspheres possess much better catalytic activity for M2 synthesis, consistent with above results shown in Figure 10. This is because MP-Cu_2O microspheres have abundant pore structure and higher surface area, which lead to the enhanced gas transportation together with more contact interface between the solid catalyst and the solid silicon, which are helpful to the formation of more active species Cu_3Si. In the Rochow reaction, Cu_3Si is normally suggested as the key catalytic active species,[51] on which M2 is formed.[52] Cu_3Si formed between the copper catalyst and the Si interface[53] is an indicator of activity for a copper catalyst.[27] Figure 11 shows XRD patterns of the contact mass before and after reaction. The contact mass is the solid mixture comprised of the reactant Si and the catalyst Cu_2O. Before the reaction, two fresh contact masses (MP-Cu_2O+Si and NP-Cu_2O+Si) exhibit the same XRD profile as shown in Figure 11a. In contrast, after the reaction, Cu and Cu_3Si species appeared in both of the reacted contact masses as shown in Figure 11b. The formation of Cu originated from the action of chlorosilane by removing the oxygen from the Cu_2O catalysts.[25] Cu and Si then will react by diffusion to form Cu_3Si. Copper then diffuses away from the Cu_2O/Cu_3Si interface. The flux of Cu is toward the Cu_3Si/Si interface, at which new Cu_3Si forms.[53] Although Cu peaks for both reacted contact masses are very similar, much higher intensity of Cu_3Si for MP-Cu_2O microspheres than for NP-Cu_2O is observed, indicating that MP-Cu_2O microspheres are more active in creating Cu_3Si than NP-Cu_2O. Large surface area and pore structure of MP-Cu_2O catalyst may encourage the alloying between Cu and Si, thus promoting the formation of active Cu_3Si phases, which is the key contribution to the enhanced catalytic activity for M2 production.

It should be mentioned that, as compared to commercial copper catalysts Cu−Cu_2O−CuO,[54] whose M2 selectivity is more than 80%,[55] MP-Cu_2O synthesized is not high enough in activity. Our intention in this work is to exploit the structure−property relationship of the copper catalysts for the Rochow reaction, because the relevant report has not been found elsewhere. Along this way, many nanostructured copper catalysts would be developed and may give way to high efficient copper catalysts.

4. CONCLUSIONS

We demonstrate a facile hydrothermal method to prepare mesoporous Cu_2O (MP-Cu_2O) and nonporous Cu_2O (NP-Cu_2O) microspheres. These Cu_2O microspheres have a diameter in the range of 100−1000 nm and surface area of about 5−65.8 m^2/g, depending on the synthesis conditions, for example, reaction temperature, time, and reactant amounts, etc. As compared to NP-Cu_2O, MP-Cu_2O shows better oxidability and reducibility. Importantly, MP-Cu_2O microspheres also exhibit better catalytic property than NP-Cu_2O for dimethyldichlorosilane synthesis via the Rochow reaction. This is because the developed pore structure within MP-Cu_2O leads to the higher oxidability and reducibility than NP-Cu_2O, together with enhanced mass transport and the more Cu−Si contact points, thus forming much more active Cu_3Si between Si and MP-Cu_2O. The work not only provides insights into the Cu catalysis in the Rochow reaction, but is also useful clue for better catalyst design.

dx.doi.org/10.1021/ie2020747 |*Ind. Eng. Chem. Res.* 2012, 51, 1264–1274

AUTHOR INFORMATION

Corresponding Author

*Tel.: +86-10-82544850. Fax: +86-10-82544851. E-mail: fbsu@mail.ipe.ac.cn.

ACKNOWLEDGMENT

We gratefully acknowledge the financial support from the Hundred Talents Program of the Chinese Academy of Sciences (CAS), CAS-Locality Cooperation Program (no. DBNJ-2011-058), State Key Laboratory of Multiphase Complex Systems (no. MPCS-2011-D-14), National Natural Science Foundation of China (no. 21031005), China Postdoctoral Science Foundation (no. 20110490597), and National Youth Foundation of China (no. 50903045).

REFERENCES

(1) Hu, L.; Peng, Q.; Li, Y. Selective synthesis of Co_3O_4 nanocrystal with different shape and crystalplane effect on catalytic property for methane combustion. *J. Am. Chem. Soc.* **2008**, *130*, 16136.

(2) Wang, H. E.; Zheng, L. X.; Liu, C. P.; Liu, Y. K.; Luan, C. Y.; Cheng, H.; Li, Y. Y.; Martinu, L.; Zapien, J. A.; Bello, L. Rapid microwave synthesis of porous TiO_2 spheres and their applications in dye-sensitized solar cells. *J. Phys. Chem. C* **2011**, *115*, 10419.

(3) Liu, Y.; Wang, D.; Peng, Q.; Chu, D.; Liu, X.; Li, Y. Directly assembling ligand-free ZnO nanocrystals into three-dimensional mesoporous structures by oriented attachment. *Inorg. Chem.* **2011**, *50*, 5841.

(4) Manna, S.; Das, K.; De, S. K. Template-free synthesis of mesoporous CuO dandelion structures for optoelectronic applications. *ACS Appl. Mater. Interfaces* **2010**, *2*, 1536.

(5) Wang, Z.; Luan, D.; Ming, C.; Su, F.; Madhavi, S.; Boey, F. Y. C.; Lou, X. W. Engineering nonspherical hollow structures with complex interiors by template-engaged redox etching. *J. Am. Chem. Soc.* **2010**, *132*, 16271.

(6) Zhang, J. T.; Liu, J. F.; Peng, Q.; Wang, X.; Li, Y. D. Nearly monodisperse Cu_2O and CuO nanospheres: preparation and applications for sensitive gas sensors. *Chem. Mater.* **2006**, *18*, 867.

(7) Musa, A. O.; Akomolafe, T.; Carter, M. J. Production of cuprous oxide, a solar cell material, by thermal oxidation and a study of its physical and electrical properties. *Sol. Energy Mater. Sol. Cells* **1998**, *51*, 305.

(8) Zhang, Y.; Deng, B.; Zhang, T.; Gao, D.; Xu, A. W. Shape effects of Cu_2O polyhedral microcrystals on photocatalytic activity. *J. Phys. Chem. C* **2010**, *114*, 5073.

(9) Zhu, H. T.; Wang, J. X.; Xu, G. Y. Fast synthesis of Cu_2O hollow microspheres and their application in DNA biosensor of hepatitis B virus. *Cryst. Growth Des.* **2009**, *9*, 633.

(10) Park, J.; Kim, J.; Kwon, H.; Song, H. Gram-scale synthesis of Cu_2O nanocubes and subsequent oxidation to CuO hollow nanostructures for lithium-ion battery anode materials. *Adv. Mater.* **2009**, *21*, 803.

(11) Zhang, L.; Wang, H. Interior structural tailoring of Cu_2O shell-in-shell nanostructures through multistep Ostwald ripening. *J. Phys. Chem. C* **2011**, *115*, 18479.

(12) Liu, H.; Ni, Y.; Wang, F.; Yin, G.; Hong, J.; Ma, Q.; Xu, Z. Fabrication of submicron Cu_2O hollow spheres in an O/W/O multiple emulsions. *Colloids Surf., A* **2004**, *235*, 79.

(13) Yang, M.; Zhang, Y.; Pang, G.; Feng, S. Preparation of Cu_2O hollow nanospheres under reflux conditions. *Eur. J. Inorg. Chem.* **2007**, *24*, 3841.

(14) Zeng, H. C.; Chang, Y.; Teo, J. J. Formation of colloidal CuO nanocrystallites and their spherical aggregation and reductive transformation to hollow Cu_2O nanospheres. *Langmuir* **2005**, *21*, 1074.

(15) Sharma, P.; Bhatti, H. Synthesis of fluorescent hollow and porous Cu_2O nanopolyhedras in the presence of poly(vinyl pyrrolidone). *Mater. Chem. Phys.* **2009**, *114*, 889.

(16) Wang, W. Z.; Xu, H. L. Template synthesis of multishelled Cu_2O hollow spheres with a single-crystalline shell wall. *Angew. Chem., Int. Ed.* **2007**, *46*, 1489.

(17) Yu, H.; Yu, J.; Liu, S.; Stephen, M. Template-free hydrothermal synthesis of CuO/Cu_2O composite hollow microspheres. *Chem. Mater.* **2007**, *17*, 4327.

(18) Singh, D. P.; Neti, N. R.; Sinha, A. S. K.; Onkar, N. S. Growth of different nanostructures of Cu_2O (nanothreads, nanowires, and nanocubes) by simple electrolysis based oxidation of copper. *J. Phys. Chem. C* **2007**, *111*, 1638.

(19) Hong, X.; Wang, G.; Zhu, W.; Shen, X.; Wang, Y. Synthesis of sub-10 nm Cu_2O nanowires by poly(vinyl pyrrolidone)-assisted electrodeposition. *J. Phys. Chem. C* **2009**, *113*, 14172.

(20) Kuo, C. H.; Huang, M. H. Facile synthesis of Cu_2O nanocrystals with systematic shape evolution from cubic to octahedral structures. *J. Phys. Chem. C* **2008**, *112*, 18355.

(21) Xu, H.; Wang, W.; Zhu, W. Shape evolution and size-controllable synthesis of Cu_2O octahedra and their morphology-dependent photocatalytic properties. *J. Phys. Chem. B* **2006**, *110*, 13829.

(22) Jimenez, C. G.; Comini, E.; Ferroni, M.; Sberveglieri, G. Synthesis of Cu_2O bi-pyramids by reduction of $Cu(OH)_2$ in solution. *Mater. Lett.* **2010**, *64*, 469.

(23) Yin, M.; Wu, C. K.; Lou, Y.; Burda, C.; Koberstein, J. T.; Zhu, Y.; Brien, S. O. Copper oxide nanocrystals. *J. Am. Chem. Soc.* **2005**, *127*, 9506.

(24) Jörg, A.; Klaus, B. Thermodynamic assessment of the copper catalyzed direct synthesis of methylchlorosilanes. *J. Organomet. Chem.* **2008**, *693*, 2483.

(25) Lewis, L. N.; Ward, W. J. These of a fixed-bed reactor to evaluate theinteractions of catalysts and promoters in the methyl chlorosilane reaction and to determine the effect of Cu in the form of the eta phase on this reaction. *Ind. Eng. Chem. Res.* **2002**, *41*, 397.

(26) Voorhoeve, R.; Geertsem, B.; Vlugter, J. C. Mechanism and kinetics of metal-catalyzed synthesis of methylchlorosilanes. *J. Catal.* **1965**, *4*, 43.

(27) Sun, D.; Bent, B. E. Chemistry of the direct synthesis of methylchlorosilanes from methyl + chlorine monolayers on a Cu_3Si surface. *Catal. Lett.* **1997**, *46*, 127.

(28) Floquet, N.; Yilmaz, S.; Falconer, J. L. Interaction of copper-catalysts and Si(100) for the direct synthesis of methylchlorosilanes. *J. Catal.* **1994**, *148*, 348.

(29) Gordon, A. D.; Hinch, B. J.; Strongin, D. R. Effects of multiple promotion of the direct synthesis contact mass with P, Zn, and Sn on the synthesis of methylchlorosilanes. *Catal. Lett.* **2009**, *133*, 14.

(30) Rochow, E. G. The direct synthesis of organosilicon compounds. *J. Am. Chem. Soc.* **1945**, *67*, 963.

(31) Voorhoeve, R.; Lips, J. A.; Vlugter, J. C. Mechanism and kinetics of the metal-catalyzed synthesis of methylchlorosilanes. *J. Catal.* **1964**, *3*, 414.

(32) Bablin, J. M.; Lewis, L. N.; Bui, P.; Gardner, M. Mechanism of the methylchlorosilane reaction: improved lab reactor design and kinetic data. *Ind. Eng. Chem. Res.* **2003**, *42*, 3532.

(33) Lyons, C. P. H.; Roussillon, G. S. Direct catalytic synthesis of dimethyldichlorosilane from methyl chloride and silicon. USP-4661613, 1987.

(34) Bablin, J. M.; Crawford, A. C.; DeMoulpied, D. C.; Lewis, L. N. Effect of low aluminum silicon on the direct process. *Ind. Eng. Chem. Res.* **2003**, *42*, 3555.

(35) Luo, W.; Wang, G.; Wang, J. Effect of CuCl particle size on the reduction reaction by silicon in preparation of contact mass used for methylchlorosilane synthesis. *Ind. Eng. Chem. Res.* **2006**, *45*, 129.

(36) Wu, Z. J.; Zhao, J. S.; Zhang, M. H.; Li, W.; Tao, K. Y. Synthesis of a stable and porous Co-B nanoparticle catalyst for selective hydrogenation of cinnamaldehyde to cinnamic alcohol. *Catal. Commun.* **2010**, *11*, 973.

(37) Zhang, X. J.; Wang, G. F.; Wu, H. B.; Zhang, D.; Zhang, X. Q.; Li, P.; Wu, H. Q. Synthesis and photocatalytic characterization of porous cuprous oxide octahedra. *Mater. Lett.* **2008**, *62*, 4363.

(38) Liang, D. D.; Liu, S. X.; Ma, F. J.; Wei, F.; Chen, Y. G. A crystalline catalyst based on a porous metal-organic framework and 12-tungstosilicic acid: particle size control by hydrothermal synthesis for the formation of dimethyl ether. *Adv. Synth. Catal.* **2011**, *353*, 733.

(39) Yang, H.; Liu, Z. H. Facile synthesis, shape evolution, and photocatalytic activity of truncated cuprous oxide octahedron microcrystals with hollows. *Cryst. Growth Des.* **2010**, *10*, 2064.

(40) Zhao, H. Y.; Wang, Y. F.; Zeng, J. H. Hydrothermal synthesis of uniform cuprous oxide microcrystals with controlled morphology. *Cryst. Growth Des.* **2008**, *8*, 3731.

(41) Luo, Y.; Li, S.; Ren, Q.; Liu, J.; Xing, L.; Wang, Y.; Yu, Y.; Jia, Z.; Li, J. Facile synthesis of flowerlike Cu_2O nanoarchitectures by a solution phase route. *Cryst. Growth Des.* **2007**, *7*, 87.

(42) Shen, Q.; Wang, H. H.; Tian, F.; Li, X. P.; Liu, F. L. Preparation and shape evolution of cuprous oxide in the solution phases of copper (II) dodecyl sulfate. *Powder Technol.* **2010**, *197*, 298.

(43) Gao, L.; Liang, X. D.; Yang, S. W.; Sun, J. Facile synthesis and shape evolution of single-crystal cuprous oxide. *Adv. Mater.* **2009**, *21*, 2068.

(44) Cao, Y.; Wang, Y.; Zhou, K.; Bi, Z. Morphology control of ultrafine cuprous oxide powder and its growth mechanism. *Trans. Nonferrous Met. Soc. China* **2010**, *20*, 216.

(45) Zhu, L. P.; Xiao, H. M.; Zhang, W. D.; Yang, G.; Fu, S. Y. One-pot template-free synthesis of monodisperse and single-crystal magnetite hollow spheres by a simple solvothermal route. *Cryst. Growth Des.* **2008**, *8*, 957.

(46) Gao, L. A.; Ha, B. P. Fabrication of Fe_3O_4 core-shell polyhedron based on a mechanism analogue to Ostwald ripening process. *J. Cryst. Growth* **2007**, *303*, 616.

(47) Shen, Y. H.; Li, S. K.; Li, C. H.; Huang, F. Z.; Wang, Y.; Xie, A. J.; Wu, Q. One-pot synthesis of uniform hollow cuprous oxide spheres fabricated by single-crystalline particles via a simple solvothermal route. *J. Nanopart. Res.* **2011**, *13*, 2865.

(48) Shen, X. H.; Chen, Q. D.; Gao, H. C. Formation of solid and hollow cuprous oxide nanocubes in water-in-oil microemulsions controlled by the yield of hydrated electrons. *J. Colloid Interface Sci.* **2007**, *312*, 272.

(49) Xu, L. S.; Chen, X. H.; Wu, Y. R.; Chen, C. S.; Li, W. H.; Pan, W. Y.; Wang, Y. G. Solution-phase synthesis of single-crystal hollow Cu_2O spheres with nanoholes. *Nanotechnology* **2006**, *17*, 1501.

(50) Guo, H. Q.; Li, D. B.; Jiang, D.; Xiao, H. C.; Li, W. H.; Sun, Y. H. Characterization and performance of V_2O_5-TiO_2 catalysts prepared by rapid combustion method. *Catal. Today* **2010**, *158*, 439.

(51) Banholzer, W. F.; Burrell, M. C. Characterization of reactive areas in the direct process for the production of methylchlorosilanes. *J. Catal.* **1988**, *114*, 259.

(52) Frank, T. C.; Kester, K. B.; Falconer, J. L. Catalytic formation of silanes on copper silicon alloys. *J. Catal.* **1985**, *91*, 44.

(53) Banholzer, W. F.; Lewis, N.; Ward, W. Active site formation in the direct process for methylchlorosilanes. *J. Catal.* **1986**, *101*, 405.

(54) Lewis, K. M.; Ritscher, J. S. Rochow-Müller direct synthesis using nanosized copper catalyst. USP-7153991, 2006.

(55) Barr, M. K.; Murphy, T. M.; Williams, M. G. Catalysts for the production of methylchlorosilanes using zinc oxide promoters. USP-7205258, 2007.